Title

Paleointensity estimates from historic and modern Hawaiian lava flows using glassy basalt as a primary source material

Authors

Cromwell, G
Tauxe, L
Staudigel, H
et al.

Publication Date

2015-04-01

DOI

10.1016/j.pepi.2014.12.007

Peer reviewed

Physics of the Earth and Planetary Interiors 241 (2015) 44–56

Contents lists available at ScienceDirect

Physics of the Earth and Planetary Interiors

journal homepage: www.elsevier.com/locate/pepi

Paleointensity estimates from historic and modern Hawaiian lava flows using glassy basalt as a primary source material

G. Cromwell [a,*], L. Tauxe [a], H. Staudigel [b], H. Ron [c]

[a] Geosciences Research Division, Scripps Institution of Oceanography, University of California San Diego, La Jolla, CA, USA
[b] Institute of Geophysics and Planetary Physics, Scripps Institution of Oceanography, University of California San Diego, La Jolla, CA, USA
[c] Institute of Earth Science, Hebrew University of Jerusalem, Jerusalem, Israel

ARTICLE INFO

Article history:
Received 5 March 2014
Received in revised form 11 October 2014
Accepted 23 December 2014
Available online 14 January 2015

Keywords:
Paleointensity
Volcanic glass
Hawaii
Geomagnetic field

ABSTRACT

Published paleointensity estimates derived from lavas extruded in known fields are highly variable and rarely recover the expected field strength within an accuracy of better than 10%. Inconsistent results on modern volcanic rocks lend even greater uncertainty to intensity experiments performed on lava flows emplaced during periods of unknown geomagnetic field strength. The majority of published paleointensity data are collected from the slowly cooled, massive centers of lava flows, where the magnetic grains are more likely to be multi-domain and produce non-ideal experimental results. Glassy volcanic material (found on subaerial lava flow tops and in sub-aqueous and subglacial environments), however is rapidly cooled, and therefore most likely of all volcanic materials to behave as single-domain particles demanded by Néel theory. We present a new paleointensity study of historic and modern Hawaiian lavas and test the viability of subaerially emplaced glassy basaltic material as an accurate recorder of magnetic field intensity. Six of eight lava flows sampled on the Big Island of Hawaii (1843, 1859, 1935, 1950, 1960, 1990 C.E.) produce well behaved Arai plots and recover an average intensity to within 2.7 μT of the expected field strength or better than 8% accuracy. We apply very strict selection criteria, including a minimum of three specimens per site, to prevent extraneous field estimates from affecting the final results. Individual volcanic glass results from the 1960 C.E. lava flow have a much lower variance than published data from the same volcanic unit. Glassy materials should therefore be collected wherever possible as they allow recovery of geomagnetic field strength with unprecedented accuracy.

1. Introduction

One of the major occupations of paleomagnetic research is characterizing the behavior of the Earth's magnetic field over time including both directional and intensity variations. Perturbations of the geomagnetic field on a global scale reveal insights into its structure on centennial (Jackson et al., 2000), millennial (e.g., Korte et al., 2009), million (e.g., Tanaka et al.,1995; Ziegler et al., 2011) and billion (Tarduno et al., 2010; Biggin et al., 2012) year timescales. Investigations into the behavior of the geomagnetic field over times scales longer than human observations are based on global compilations of paleomagnetic data and are dependent on the accuracy of available paleodirection and paleointensity estimates. Paleointensity estimates come from a variety of sources, including deep sea sediments, volcanic rocks and archeological artifacts. Volcanic rocks have the advantage over other materials that they may provide absolute intensity estimates from present day to hundreds of millions and perhaps billions of years ago. However, the ability of lava flow samples to accurately record the strength of the ancient magnetic field may affect our understanding of geomagnetic field behavior.

There are many experiments designed to recover the paleointensity signal from volcanic rocks (see Tauxe and Yamazaki (2007) for an in depth review). Some of the most widely used methods are the Königsberger-Thellier–Thellier technique (Königsberger, 1938; Thellier and Thellier, 1959) and its derivatives (e.g., Coe, 1967; Aitken et al., 1988; Hill and Shaw, 1999; Tauxe and Staudigel, 2004), the Shaw method (Shaw, 1974) and its variants (e.g., Tsunakawa and Shaw, 1994), and multispecimen approaches (e.g., Hoffman et al., 1989; Hoffman and Biggin, 2005; Deckers and Böhnel, 2006). Each experiment is tested against modern lava flows erupted in known fields where the null hypothesis that volcanic rocks cannot accurately record magnetic field strength is disproven when the measured specimens agree with the known field intensity (within error). Love and Constable (2003) analyzed the reliability of all available intensity data from

* Corresponding author.

http://dx.doi.org/10.1016/j.pepi.2014.12.007
0031-9201/

the 1960 Kilauea lava flow from the Big Island of Hawaii and found an average field strength of 33.91 μT with a standard deviation of 19% (expected intensity = 36.0 μT). Herrero-Bervera and Valet (2009) made their own compilation of the same flow and confirmed that the majority of published intensity estimates do not consistently recover the expected field strength, especially those estimates derived from Thellier-type experiments. Some individual results from this method differ by more than 50%. Failure to consistently reproduce a known field is troubling when considering the importance of paleointensity results in geomagnetic field modeling.

The stark disagreement among paleointensity results from the same cooling unit can be attributed to different experimental techniques, varying selection criteria between researchers, and the degree to which specimens alter or multi-domain behavior (Yamamoto et al., 2003; Chauvin et al., 2005). Yamamoto (2006) also suggest that overestimates of field strength could be caused by acquisition of thermochemical remanent magnetization (TCRM) during lava flow emplacement. With few exceptions, paleointensity methodologies are based on the assumption that the measured specimens are comprised of single-domain magnetic grains and that there is a linear relationship between the ancient magnetic field and the imparted laboratory field. The majority of paleointensity studies, however, sample a range of grain sizes from single-domain (<80 nm) to pseudo-single-domain (∼100 nm) and multi-domain (>∼200 nm) (Tauxe et al., 2010), so often illustrated in Day plots (Day et al., 1977). Multi-domain specimens produce non-linear, Arai plots (Levi, 1977; Dunlop and Özdemir, 2001) which require subjective NRM/TRM slope interpretations. The failure of many Thellier-type historical measurements may have less to do with experimental methods or loose selection criteria, but rather that researchers collect their samples from the slowly cooled interiors of lava flows where crystals are more massive, and multi-domain grains will have a greater influence on the remanent magnetization of the volcanic rock.

An alternate strategy would be to target rapidly cooled, fine grained material for paleointensity studies (e.g., Pick and Tauxe, 1993; Bowles et al., 2006) where experimental results are more likely to be well behaved, rather than interpret or attempt to correct for multi-domain behavior after the fact (e.g., Deckers and Böhnel, 2006; Wang and Kent, 2013). Subaerial rhyolitic volcanic glass has been tested as a suitable recorder of paleointensity (e.g., Leonhardt et al., 2006; Ferk et al., 2012) in relation to laboratory (Ferk et al., 2010) and ancient (Ferk et al., 2011) magnetic fields. Here, we explore the viability of glassy margins of subaerial lava flows as recorders of magnetic field strength. We collected quickly cooled, glassy volcanic material from eight historic lava flows on the Big Island of Hawaii and compared our paleointensity results to the expected field strength. The intensity for historic lavas is well known from the International Geomagnetic Reference Field model (IGRF) (1900 C.E. to present). Prior to 1900, models such as GUFM (Jackson et al., 2000), ARCH3k and CALS3K (Korte et al., 2009) provide reasonable estimates of the expected field.

2. Methods

2.1. Sampling

We sampled rapidly-cooled volcanic material from eight historic basaltic lava flows on the Big Island of Hawaii (Fig. 1). Unoriented hand samples were collected using a rock hammer and chisel from carefully selected sections of each lava flow. We collected volcanic glass on pahoehoe ropes from the 1843, 1859, 1935, 1990 and 2010 (Fig. 1b) C.E. flows, and aa spires from the 1907, 1950 and 1960 (Fig. 1 C.E. flows. Care was taken to avoid areas with signs of alteration or complicated cooling structures. At each locality we collected at least two samples from different surfaces in order to increase the probability of acquiring reliable paleointensity results and obtain an internal consistency check for paleointensity results.

2.2. Paleointensity

Rapidly cooled material was subsampled from larger hand samples in the laboratory. Specimens with magnetic moments of at least 10^{-10} Am^2 were subjected to ultrasonic treatment to remove any superficial dirt or alteration features that might acquire a thermal magnetic signature during laboratory heatings. During the ultrasonic treatment, all specimens were placed in beakers with a 10% HCl solution in a water bath for 15 minutes. The ultrasonic bath was chilled to prevent the specimens from heating above 30°C and potentially acquiring a partial thermal remanent magnetization (pTRM). Following ultrasonic cleaning, all specimens were placed in labeled glass tubes for the paleointensity heating experiment.

We used the IZZI-modified Thellier–Thellier experiment (Tauxe and Staudigel, 2004) to estimate field strength from 131 specimens

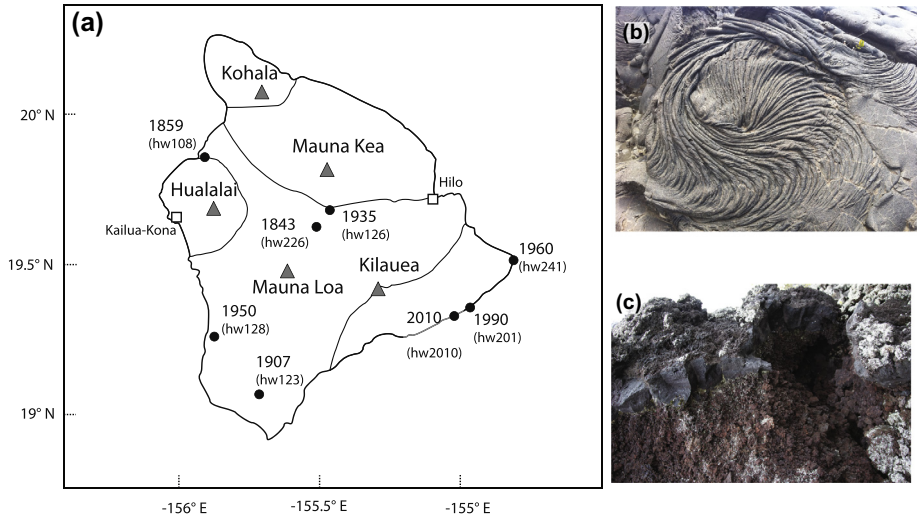

Fig. 1. (a) Sample locations of historic Hawaiian lava flows on the Big Island. Lava flow ages are years, C.E., and site names are listed in parentheses. Volcanic centers are plotted as triangles along with the general surface geology cover for each volcano. (b) Photo of 2010 lava flow sampling site. (c) Photo of 1950 sampling site.

Table 1
Selection statistics at the specimen and site level and their threshold values. For *SCAT*, the $\beta_{threshold}$ value is 0.1. See text for a brief definition of each statistic.

			Specimen			
SCAT	*FRAC*	*Gap Max*	β	MAD_{free}	*DANG*	$\lvert\vec{k}\rvert$
TRUE	$\geqslant$0.78	$\geqslant$0.60	$\leqslant$0.10	$\leqslant$5.0°	$\leqslant$10.0°	$\leqslant$0.164
			Site			
nn	B_σ	B_σ %				
$\geq$ 3	$\leqslant$4 μT	$\leqslant$10 %				

from our eight historic lava flows. Step-wise heating experiments were performed in custom-built ovens at the Scripps Institution of Oceanography paleomagnetics laboratory at the University of California, San Diego. Natural remanent magnetization (NRM) and pTRM measurements were taken using a 2G Cryogenic Magnetometer. A 20 μT laboratory field was applied to all specimens during in-field heating steps and pTRM alteration checks were performed at every other temperature step. IZZI experiments were carried out until at least 95% of the NRM was removed.

2.3. Selection criteria

Data interpretation was performed using the Thellier GUI Auto Interpreter of Shaar and Tauxe (2013) (part of the *PmagPy* software distribution available at http://earthref.org/PmagPy/cookbook) which provides objective and reproducible interpretations based on a uniform set of criteria. The selection statistics used in this study are listed in Table 1 and described below (for a thorough review of all paleointensity statistics see Paterson et al. (2014)).

SCAT (Shaar and Tauxe, 2013) tests the degree of scatter over a range of NRM/TRM data points and is designed to evaluate the degree of alteration or scatter about the best-fit slope. It is a boolean statistic which uses the threshold value of β (in this case $\beta_{threshold}$ = 0.1, see below) to test whether experimental measurements on the best-fit Arai plot (Nagata et al., 1963) are too scattered. There is no absolute numerical requirement for *SCAT*, instead the criterion is labeled *True* if all points associated with a chosen Arai plot segment fall within the *SCAT* polygon (illustrated graphically in e.g., Fig. 2a). *FRAC* (Shaar and Tauxe, 2013) measures the fraction of the NRM used in calculating a paleointensity value. *FRAC* is calculated from the NRM fraction of a select range of NRM/TRM data points on an Arai plot and is determined using the full vector difference sum calculation. *Gap Max* (Shaar and Tauxe, 2013) is the maximum gap between two NRM/TRM data points determined by vector arithmetic. β (Coe et al., 1978; Tauxe and Staudigel, 2004) measures the relative scatter around the best-fit line in an Arai plot. It is defined as the ratio of the standard error of the slope to the absolute value of the slope. *DANG* (Tauxe and Staudigel, 2004), or Deviation ANGle, is the angular difference between the NRM components used in the best-fit line and the angle that the line anchoring the center of mass makes with the origin. MAD_{free} (Kirschvink, 1980) (maximum angle of deviation) is a measure of scatter about the best-fit line through the NRM steps in an Arai plot. We also calculated the curvature statistic, $\vec{k}$, of Paterson (2011). Curvature is calculated by using a least squares approach to fit the data in an Arai plot with a best-fit circle of the form $(x-a)^2+(y-b)^2=r^2$ (Taubin, 1991; Chernov and Lesort, 2005), where x is the TRM gained and y is the NRM remaining. $\vec{k}$ is the inverse of the calculated radius, $1/r$. A more curved arc has a higher value of $\vec{k}$ and a perfectly straight line will have a $\vec{k}=0$. We calculated $\vec{k}'$, which is a measure of the curvature over a select range of temperature steps, not the complete Thellier experiment.

As a first pass, we chose *MAD*, *Gap Max*, and *DANG* to be relatively strict (5°, 0.6 and 10° respectively) while the Thellier Consistency Test tool was used to select values for *FRAC* and β. The Thellier Consistency Test (part of the Thellier GUI package) varies *FRAC* and β and calculates a range of paleointensity results from the entire suite of specimen measurements while keeping *MAD*, *Gap Max* and *DANG* constant. Our strategy was to find the set of threshold values for β and *FRAC* that accepts the most sites with a minimum of three specimens and with a standard deviation less than 4 μT or 10% of the site mean. These strict criteria ensure that sites with poorly determined field estimates are excluded from the final analysis.

2.4. Anisotropy

Most successful specimens underwent correction for anisotropy, using either thermal (ATRM) or anhysteretic (AARM) methods. ATRM experiments included seven heating steps carried out at 550 °C. Six in-field steps were carried out in a 40 μT field at orthogonal directions (+x, +y, +z, −x, −y, −z) followed by an additional in-field alteration check at the end of the experiment (+x). AARM tensor determinations were carried out in nine measurement positions as defined by Jelinek (1978) (1–3, 6–8, and 11–13), using an alternating current peak field of 180 mT and a 100 μT direct current field. Prior to each ARM step, a baseline was established by demagnetizing each specimen in an alternating field of 180 mT. This baseline measurement was subtracted from the subsequent in-field ARM measurement.

We used an F-test (Hext, 1963) whereby the anisotropy tensor is not used if the F-test is below the threshold value for anisotropy at the 95% confidence level. ATRM and AARM tensors were applied to the final paleointensity result of each appropriate specimen (Veitch et al., 1984). Thirteen specimens passed the F-test with results above the threshold value, and the anisotropy corrections for most specimens were minimal. The average correction is about 3.5% with one specimen changing by 32% of its original intensity value (Table 2). Site accuracy and scatter improved or stayed the same for all sites with anisotropy corrections, indicating that we have effectively applied this methodology to our specimens (Paterson, 2013).

2.5. Hysteresis loops and first order reversal curves

Selected specimens were chosen for hysteresis and first order reversal curve (FORC) experiments. Hysteresis and FORC measurements were performed at the Scripps Institution of Oceanography on a Princeton Measurements Corp. Micromag Model 2900 alternating field magnetometer (AFM). FORC data were analyzed using the *FORCinel* software of Harrison and Feinberg (2008). Smoothing factors for each FORC were determined using the optimization routine in *FORCinel*.

3. Results

The majority of specimens subjected to the IZZI experiment exhibit either linear Arai plots with good reproducibility of pTRM check steps or have obvious signs of failure due to failure of pTRM check steps, or curved Arai (Nagata et al., 1963) or Zijderveld (Zijderveld, 1967) plots. Representative specimens from the IZZI paleointensity experiment and their hysteresis behavior are shown in Fig. 2. The paleointensity data are shown using the NRM versus pTRM Arai plots, with inset Zijderveld diagrams (Fig. 2a, d, g, i). Also shown are associated hysteresis loops (Fig. 2j) and successful FORC diagrams (Fig. 2c, f). Fig. 2a and d, are very well behaved specimens with linear Arai diagrams through the entire TRM

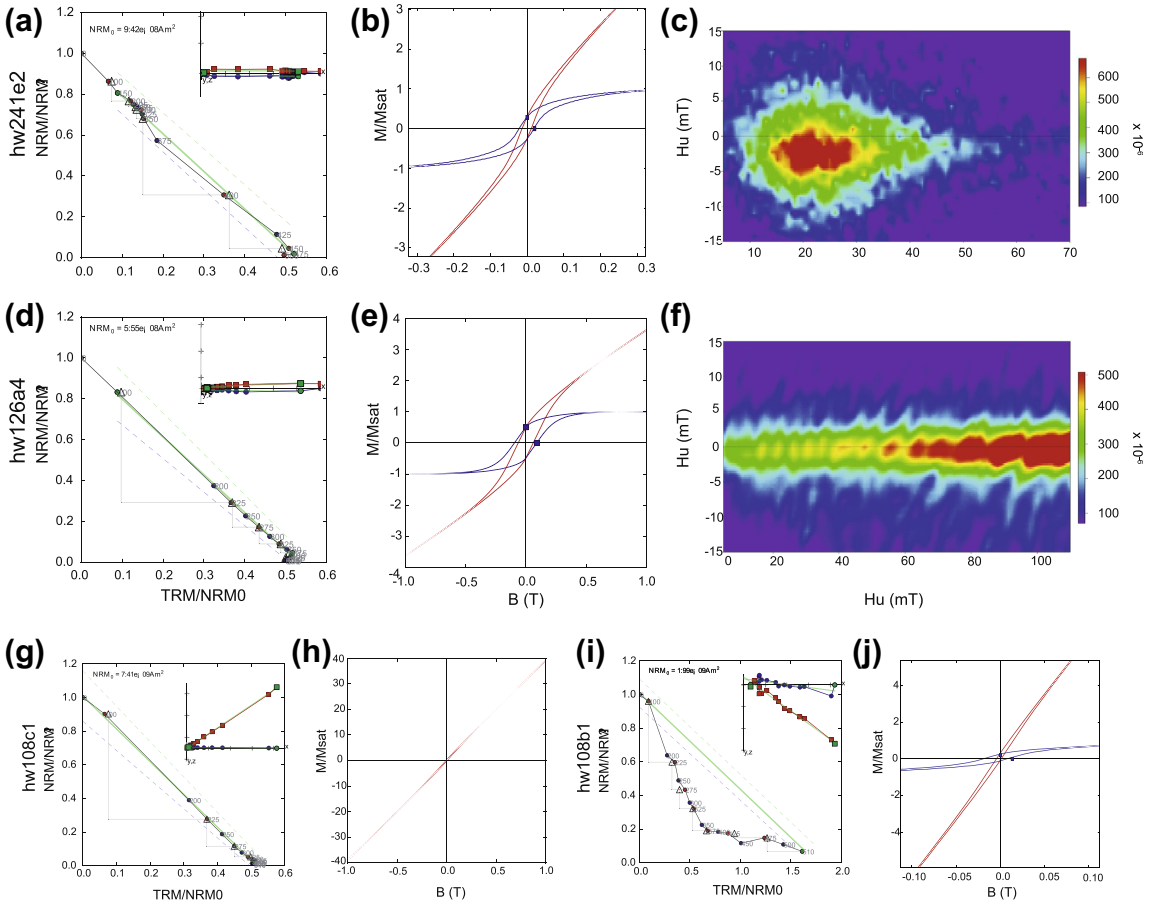

Fig. 2. Results from representative specimens in this study. Arai plots from IZZI-modified Thellier–Thellier experiments with inset Zijderveld diagrams (a, d, g, i). In the Arai plots, temperature values are listed in degree Celsius, pTRM checks are shown as triangles, zero-field/in-field temperature steps shown as red dots, in-field/zero-field steps shown in blue. The green line is the least-squares component for selected temperature steps. Hysteresis loops (b, e, h, j) show the raw hysteresis data (red) and the resulting loop after paramagnetic slope corrections. First-order reversal curve (FORC) diagrams (c, f) are produced using the *FORCinel* program of Harrison and Feinberg, 2008. Smoothing factors (SF) are listed for each specimen. (For interpretation of the references to color in this figure legend, the reader is referred to the web version of this article.)

spectrum. These specimens produce paleointensity estimates that are within <1 μT of the expected field (Table 2). Hysteresis loops for specimens hw241e2 and hw126a4 (Fig. 2b, e,) are indicative of single-domain behavior expected from quenched volcanic material. FORC distribution plots are another way to analyze hysteresis data and determine magnetic grain size. First-order reversal curve densities, from hysteresis measurements on specimens hw241e2 and hw126a4, are shown as contour plots in Figs. 2c, and f. Both plots have FORC densities concentrated along the flipping field ($\mu_0 H_u$=0) at high coercivities (H_c), indicating that a large percentage of grains are uniaxial-single domain with high coercivity values.

Specimen hw108c1 (Fig. 2g, h) also exhibits a near-linear Arai plot and records a paleointensity within 2% of the expected field strength. The hysteresis loop for this specimen, however, suggests a strong paramagnetic contribution and the FORC measurement (not shown) had no discernible signal. In this instance, rock magnetic experiments would not be a good predictor of paleointensity success as the IZZI experiment for hw108c1 passes all quality checks and accurately recovers the expected magnetic field strength. A different specimen from the same lava flow, hw108b1 (Fig. 2i, j), is not single-domain, as evidenced by the concave-up Arai plot. There is also a substantial paramagnetic contribution (Fig. 2j), but the FORC diagram (not shown) was not recoverable without a very large smoothing factor (SF = 10).

A scanning election microscope (SEM) image from hw108c2 (Fig. 3a) shows that the primary magnetic carrier for this specimen is micrometer-scale dendritic titanomagnetites. Similarly sized titanomagnetite dendrite structures are found in hw2010B (Fig. 3c-f) where Shaar and Feinberg (2013) observed fine dendrites arranged along the edges of larger pyroxene grains in the glass. Dendritic textures dominate these Hawaiian glasses, but there is still a large population of non-dendritic titanomagnetites (Shaar and Feinberg, 2013) that may contribute to the natural remanence.

A total of 54 out of 131 specimens (41%), representing six of our eight sampled lava flows, pass our optimized experimental requirements listed in Table 1. Specimen paleointensity results and accompanying statistics are listed in Table 2 and averages for each lava flow are listed in Table 3. All listed intensity values are corrected for anisotropy if those experiments passed an anisotropy F-test (Hext, 1963).

Average site intensities for each successful lava flow are consistent with the expected magnetic field strength in Hawaii. Five of six flows recover the historic field intensity to within 10% of the expected value (Table 3 and Fig. 4), and four of these are within 4%. The 1990 (hw201) and the 2010 (hw2010B) flows have average field strengths at least 8% lower than the expected field.

Paleointensity results from the 1907 flow (site hw123) exceed the variance limit set in our site level criteria. The circumstances surrounding this site rejection are curious because all six measured specimens pass the optimum specimen level criteria, but one specimen, hw123a9, records an intensity value of 90.2 μT, nearly three times the expected field strength (37.8 μT) and no anisotropy correction was applied because the F-test determined that the

Table 2
Paleointensity results from historical Hawaiian lava flows that meet our optimized selection criteria. Field estimates derived from IZZI-modified Thellier–Thellier paleointensity experiments and calculated using the Thellier GUI Auto Interpreter. Listed beneath Lava Flow are the year of emplacement, latitude, longitude and the expected field intensity, B_{exp} from the IGRF or ARCH3K models. B_F is the estimated field strength based on $T°C$ temperature intervals. A_{Fac} is the ratio of anisotropy corrected/uncorrected intensity. Experimental statistics: *FRAC*, β, *MAD*, *DANG* and $\vec{k}'$. Specimens that would fail the $|\vec{k}'|$ criterion are indicated with a *. See text for information on site means hw108x and hw123x.

Lava Flow	Specimen	B_F	A_{Fac}	$T°C$	*FRAC*	β	*MAD*	*DANG*	$\vec{k}'$
1843	hw226a3	39.9	–	0–500	0.98	0.012	2.7	1.7	−0.02
B_{exp}=	hw226a5	35.45	–	0–250	0.84	0.05	2.84	0.36	0.178*
39.9 μT	hw226b2	41.53	0.99	0–400	0.82	0.01	2.8	5.88	−0.044
19.6382°N	hw226b3	38.58	–	100–500	0.88	0.03	2.67	2.31	0.05
155.5116°W	hw226b4	39.32	1.07	0–450	0.82	0.05	3.87	4.3	0.201*
	hw226b6	40.64	–	0–375	0.78	0.02	1.8	5.91	0.054
	hw226 39.2 ± 2.1 μT, *n* = 6								
1859	hw108a1	39.6	0.68	0–475	0.92	0.026	3	2.3	0.056
B_{exp}=	hw108a2	38.2	–	0–375	0.79	0.02	2	5.3	0.089
39.3 μT	hw108a3	54.1	–	0–450	0.82	0.049	3.9	4.5	−0.371*
19.8627°N	hw108a4	40.3	–	0–400	0.8	0.028	2.1	2.5	0.198*
155.9085°W	hw108a5	41.8	–	100–450	0.87	0.014	0.7	1.1	−0.047
	hw108c1	38.94	–	0–425	0.98	0.01	0.66	1.14	0.074
	hw108c2	40.02	–	100–400	0.87	0.02	0.34	0.1	−0.018
	hw108c7	38.29	–	0–375	0.9	0.02	1.84	0.77	−0.008
	hw108c8	38.44	–	0–300	0.78	0.03	2.46	4.18	0.004
	hw108c9	37.81	–	0–500	0.99	0.01	1.88	0.8	−0.025
	hw108c12	34.39	–	100–375	0.8	0.06	1.52	0.9	0.074
	hw108c13	39.01	–	0–400	0.94	0.01	1.36	0.97	−0.017
	hw108 40.3 ± 4.7 μT, *n* = 12								
	hw108x 38.8 ± 1.9 μT, *n* = 11								
1907	hw123a1	33.5	–	0–450	0.79	0.022	3.3	4.7	0.178*
B_{exp}=	hw123a2	38.2	–	100–525	0.96	0.037	1.3	0.8	−0.386*
37.7 μT	hw123a3	31.7	–	0–510	0.98	0.023	3.7	2.2	0
19.07262°N	hw123a4	35.3	–	0–510	0.96	0.034	1.5	0.5	−0.131
155.7141°W	hw123a5	36.3	–	0–450	0.83	0.052	2.3	2.1	0.412*
	hw123a9	90.2	–	150–500	0.81	0.052	3.4	1.2	0.033
	hw123 44.2 ± 22.6 μT, *n* = 6								
	hw123x 35.0 ± 2.5 μT, *n* = 5								
1935	hw126a1	36.05	–	0–400	0.98	0.01	1.28	1.89	0.118
B_{exp}=	hw126a2	35.5	–	0–325	0.82	0.034	1.9	4.2	0.269*
36.4 μT	hw126a3	30.08	–	0–350	0.8	0.03	1.51	3.47	0.202*
19.6856°N	hw126a4	37.04	–	100–375	0.78	0.02	1.9	3.6	0.112
155.4645°W	hw126a5	35.7	–	0–275	0.88	0.005	1.1	2.5	0.008
	hw126b1	35.6	–	100–425	0.84	0.015	1	1.3	0.062
	hw126b2	36.2	1.04	100–400	0.81	0.016	0.8	0.7	0.092
	hw126b3	35.6	–	0–425	0.97	0.012	0.8	1.1	0.056
	hw126b4	36.95	–	0–375	0.92	0.01	0.93	1.41	0.089
	hw126b5	36.5	–	0–375	0.92	0.008	0.5	0.4	0.016
	hw126 35.5 ± 2.0 μT, *n* = 10								
1950	hw128a1	35.34	–	0–350	0.83	0.018	2.8	4.2	−0.111
B_{exp}=	hw128a2	37.42	–	100–510	0.89	0.02	1.43	1.72	0.138
36.2 μT	hw128a3	35.09	–	100–475	0.87	0.033	1.9	2.6	0.2
19.2641°N	hw128a4	36.08	1	200–510	0.8	0.02	0.83	1.35	0.197*
155.8743°W	hw128a5	35.61	–	200–510	0.78	0.03	0.79	0.43	0.222*
	hw128a6	36.6	–	100–500	0.87	0.04	1.62	2.52	0.084
	hw128a7	28.87	1.02	100–425	0.83	0.02	1.89	2.61	−0.141
	hw128a8	34.9	–	0–375	0.83	0.02	2.6	0.5	−0.125
	hw128a9	31.8	–	0–425	0.85	0.014	1.9	2.7	0.016
	hw128a10	32.53	1.06	150–425	0.78	0.02	2.23	3.14	−0.083
	hw128a11	43.75	–	150–500	0.85	0.03	1.47	2.04	0.171*
	hw128b3	29.6	–	200–510	0.79	0.02	4.7	1.7	0.028
	hw128b4	31	–	200–510	0.88	0.019	2.9	0.8	0.058
	hw128b5	38.1	–	300–500	0.8	0.036	3	2.8	0.195*
	hw128c1	34.02	1.06	0–510	1	0.01	2.27	0.75	0.053
	hw128c2	32.73	0.96	225–510	0.79	0.01	0.85	0.15	−0.122
	hw128c3	34.9	1.05	100–500	0.96	0.009	1.3	0.6	0.02
	hw128c4	34.9	0.96	0–500	1	0.016	2.5	0.5	0.061
	hw128c5	35.13	–	200–475	0.79	0.02	1.17	0.17	−0.083
	hw128d1	36.12	0.92	100–400	0.88	0.02	2.23	2.72	0.064
	hw128d2	34.8	1.01	0–450	0.97	0.027	1.5	2.6	0.08
	hw128d3	35.49	–	0–425	0.92	0.04	1.72	4.95	0.1
	hw128d4	33.59	–	0–350	0.8	0.02	1.47	1.68	−0.098
	hw128d5	34.56	–	0–425	0.93	0.04	2.5	6.16	−0.289*
	hw128 34.7 ± 3.0 μT, *n* = 24								
1960	hw241a2	31.2	–	150–500	0.8	0.023	4.1	1.3	−0.3
B_{exp}=	hw241d3	41.4	–	275–500	0.79	0.019	4.8	2.1	0.101
36.0 μT	hw241e1	36.29	1.01	0–425	0.84	0.03	2.27	3.73	−0.134
19.51591°N	hw241e2	36.83	–	150–475	0.79	0.02	2.45	2.95	0.092

Table 2 (*continued*)

Lava Flow	Specimen	B_F	A_{Fac}	T °C	*FRAC*	β	*MAD*	*DANG*	$\vec{k}'$
154.8098°W	hw241e4	37.8	1.02	100–500	0.78	0.013	2.8	3.7	−0.005
	hw241e5	35.32	–	0–425	0.89	0.03	3.76	3.34	0.143
	hw241e6	33.92	–	0–425	0.86	0.04	2.54	2.48	0.039
	hw241 36.1 ± 3.2 μT, *n* = 7								
1990	hw201a3	34.31	–	0–325	0.79	0.03	2.68	8.79	0.163
B_{exp}=	hw201a6	32.44	–	0–500	0.95	0.02	2.45	2.04	0.21*
35.2 μT	hw201a11	31.59	–	0–400	0.81	0.03	3.34	1.37	0.159
19.3622°N	hw201a12	31.83	–	0–450	0.79	0.02	2.78	7.69	0.115
154.9666°W	*hw201 32.5 ± 1.2* μT, *n* = 4								
2010	hw2010Bb	30.4	–	0–500	0.86	0.042	3	1.9	−0.271*
B_{exp}=	hw2010Bc	28.2	–	0–500	0.8	0.07	4.6	6.6	−0.201*
34.7 μT	hw2010Be	29.9	–	0–500	0.98	0.053	2.3	3.3	−0.324*
19.35°N	*hw2010B 29.5 ± 1.2* μT, *n* = 3								
155.98°W									

specimen was not anisotropic. The other five specimens have an average intensity of 35.0 ± 2.5 μT. Some yet unknown mechanism unique to hw123a9 produced an exceptionally high magnetic field compared to its sister specimens and perhaps rejection of this specimen could be justified. Unfortunately, there is no concrete basis on which to exclude it apart from its abnormally high field. We therefore must reject the entire site from further discussion even though an argument could be made that this site, with five consistent specimens, warrants inclusion in the final analysis. The 1859 flow (site hw108) also exceeds the site level variance, with a single sample responsible for the large standard deviation. This sample (hw108a3) passes our optimized selection criteria but has a large curvature value ($\vec{k}'$ = −0.371), which, as we indicate below, may introduce a bias in site and sample level paleointensity estimates.

Concave-up Arai plots like that shown in Fig. 2i allow paleointensity interpretations from several slopes. It is possible that the "correct" paleointensity is recoverable in the Arai plot, but identifying the correct slope is highly unlikely unless the target paleointensity is known. Paleointensity estimates derived from the full experimental TRM should theoretically recover the ancient field strength (Dunlop and Özdemir, 2001), but we will show that this process consistently underestimates the expected field intensity in our experiments.

The Thellier GUI Auto Interpreter ensures that all specimens are objectively chosen to meet a certain set of selection criteria. Our strict requirements ensure that no strongly concave-up specimens are accepted (e.g., Fig. 2j), but we do observe a range of "near-ideal" Arai diagrams that are not perfectly linear (e.g., Fig. 2a) yet pass our selection criteria. Cromwell et al. (2013) observed that when the complete TRM is measured, paleointensity estimates obtained by fitting a straight line to the endpoints of curved Arai plots underestimate magnetic field intensity compared to ideally behaved sister specimens. Based on this observation we investigate whether or not specimens with even slightly concave-up Arai diagrams have lower intensity estimates than those that are more linear.

In their evaluation of Arai plot curvature and historic paleointensity estimates, Paterson (2011) observed that specimens with $|\vec{k}| < 0.164$ yielded more accurate results with lower scatter. In Fig. 5a we plot curvature for each of our accepted specimens against normalized paleointensity (B_F/B_{exp}) and evaluate the behavior of our specimens relative to the curvature threshold set by Paterson (2011). Fifteen optimized specimens have $|\vec{k}'|$ values greater than 0.164 (starred in Table 2). Removing the 15 specimens that exceed the curvature threshold slightly improves dataset accuracy and reduces scatter; the median normalized intensity improves from 0.971 to 0.974 of the expected intensity and the median absolute deviation decreases from 0.038 to 0.036. Application of $|\vec{k}'|$ as an additional selection criterion removes a small low-field bias in our dataset and is particularly important in sites where all specimens have large curvature values, such as hw2010B. The site mean intensity of hw2010B, 29.5 μT, underestimates the expected field strength by more than 15%. This low-field estimate is therefore likely to be caused by the bias introduced by curved Arai plots because all three specimens in this site have curvature (absolute) values greater than 0.164. It is evident that paleointensity data derived from specimens with $|\vec{k}'| \geqslant 0.164$ introduce a slight bias into site mean results, and that our specimen's acceptance method can be improved by applying $|\vec{k}'|$ as an additional selection requirement.

We re-ran the Thellier GUI Auto Interpreter with the added selection criterion of $|\vec{k}'| < 0.164$. A total of 59 specimens from six sites passed this strict set of criteria (Table 4, Table 5, Fig. 6). As expected, the overall accuracy of the data improved relative to our optimized, less rigorous, dataset. The median normalized intensity of all specimens increased to 0.980 and the median absolute deviation of decreased to 0.035. The most significant difference between data sets is the acceptance of site hw108 and the rejection of site hw2010B. Two specimens from hw108 (hw108a43 and hw108a4) exceeded the curvature threshold and were rejected, reducing the standard deviation to within 5% of the site mean. No specimens from site hw2010B passed the strict selection criteria. Site mean intensities and standard deviations for the remaining sites remain essentially unchanged.

While the criterion of demanding that $|\vec{k}'| < 0.164$ does increase the accuracy of our results, reducing the low bias associated with curved Arai plots, the results from the 1990 flow remain low. A low average intensity for the 1990 flow is not unique to our experiments. de Groot et al. (2013) also observe a lower than expected average field strength for this lava flow using a pseudo-Thellier method (Tauxe et al., 1995), calibrated using the 1990 flow among other historical flows. We note that their result agrees with the expected field strength (as it was designed to do) within their larger 1σ-error (33.6 ± 3.3 μT compared to 32.5 ± 1.2 μT from this study). While on location in Hawaii, we measured the local magnetic field at a number of localities and observed magnetic anomalies up to around 10% of the expected field strength. It is possible that our site results could be affected by a local field anomaly, perhaps like the 1990 flow, but the fact that most of our sites are consistent with expected field strength suggests that local magnetic anomalies are minimal.

4. Discussion

Subaerial volcanic glasses from historic lava flows allow recovery of intensities within 8% of the expected Earth's magnetic field

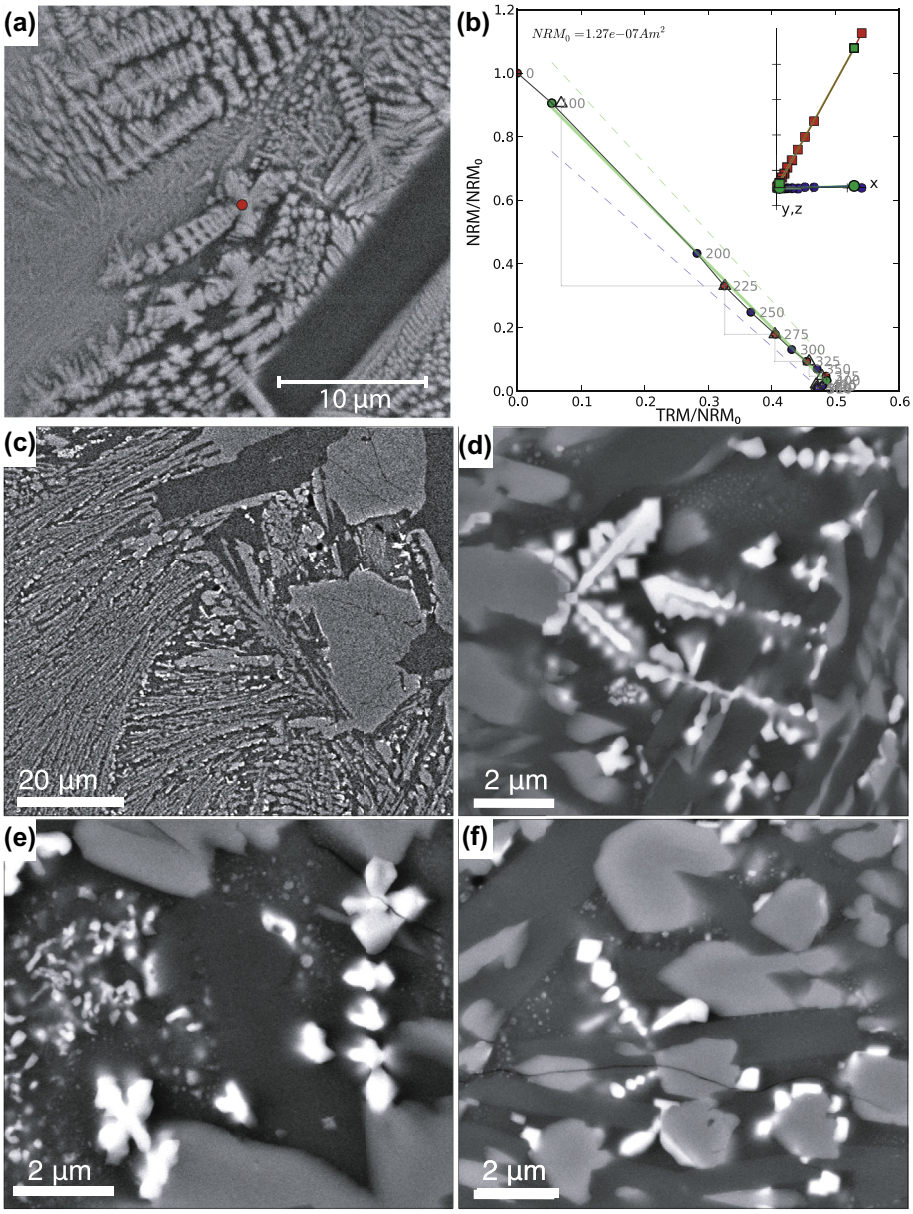

Fig. 3. (a) Backscatter scanning electron microscope image of specimen hw108c2 (1859 C.E. lava flow), a single-domain-like specimen. The red dot is the analysis target area. (b) Arai plot of the same specimen with inset Zijderveld diagram. The recovered paleointensity from this specimen is 38.94 μT and the expected field intensity for the 1859 flow is 39.29 μT. (c–f) SEM backscatter images of quenched margins from sample hw2010B (Shaar and Feinberg, 2013).

Table 3
Site level paleointensity results using optimized selection criteria for historic Hawaiian lava flows. Sample latitude and longitude listed with n specimens per site. B_F is the estimated ancient field strength in microTesla, B_σ is the standard deviation of each sample field estimate and B_σ % is percent error of each estimate. B_{exp} is the expected intensity for each lava, ΔB is the difference between the estimated and expected field strengths, ΔB% is the percent difference.

Lava flow	Site name	n	B_F (μT)	B_σ	B_σ %	B_{exp} (μT)	ΔB	ΔB%
Optimized results (without $\vec{k}'$ criterion)								
1843	hw226	6	39.2	2.1	5.4	39.2	0.0	0.0
1935	hw126	10	35.5	2.0	5.6	36.6	−1.1	−3.0
1950	hw128	24	34.7	3.0	8.6	36.3	−1.6	−4.4
1960	hw241	7	36.1	3.2	8.9	36.2	−0.1	−0.3
1990	hw201	4	32.5	1.2	3.7	35.4	−2.9	−8.2
2010	hw2010	3	29.5	1.2	4.1	34.8	−5.3	−15.2

(Fig. 4) and within 4% when applying the $\vec{k}'$ requirement. Paterson et al. (2012) considered the effect of experimental noise on Thellier-type paleointensity data and predicted that noise led to a best-case accuracy of 6–7%. We find that strict selection criteria coupled with careful sampling of rapidly cooled materials can yield sites that exceed this predicted accuracy. Our results prove that basaltic volcanic glass is an ideal material for Thellier-type paleointensity experiments. Although unoriented samples from flow tops

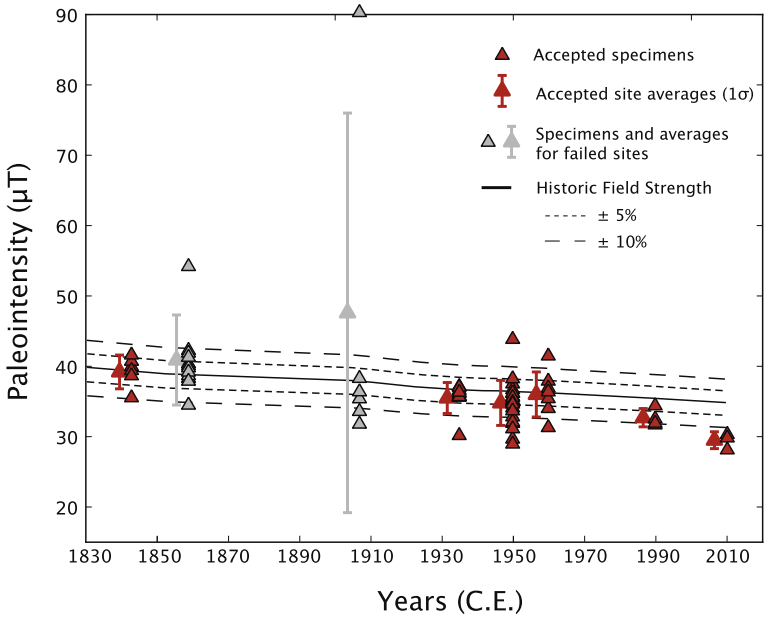

Fig. 4. Optimized specimen results from this study (red triangles), and site averages (offset) with 1σ-error bars. Sites and specimens that do not pass all selection criteria are shown in gray. Expected historic field strength for the Big Island is plotted as a solid line with 5% and 10% bounds. Hawaiian field strength calculated from D/IGRFs for 1900 to 2010 C.E. (Malin and Barraclough, 1981), prior to 1900 C.E. calculated from ARCH3K.1 (Korte et al., 2009). Field strength values were generated using igrf.py (part of Lisa Tauxe's PmagPy package). (For interpretation of the references to color in this figure legend, the reader is referred to the web version of this article.)

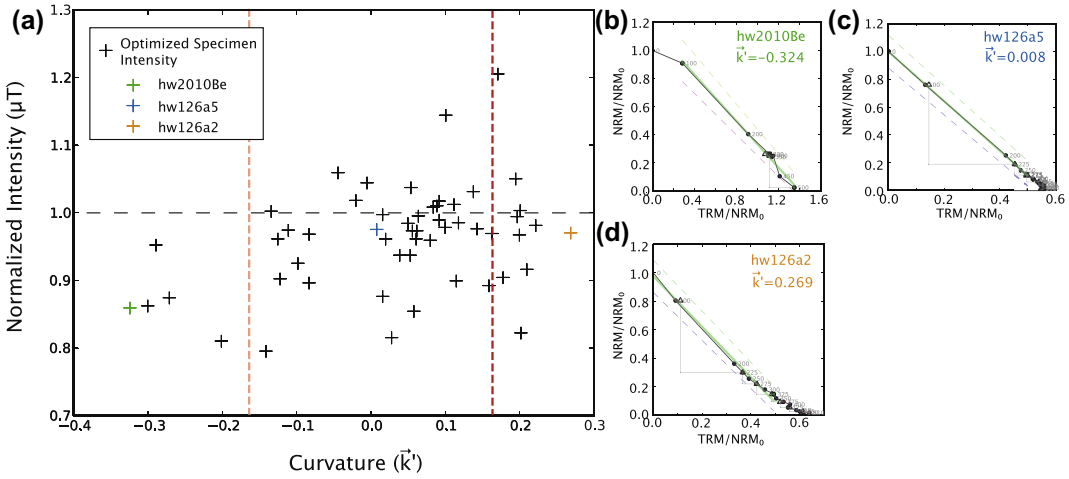

Fig. 5. (a) Curvature statistic, $\vec{k}'$, of our optimized specimens. Specimen curvature is plotted against intensities normalized against the expected field strength. The vertical dark red dashed line is the $\vec{k}'$ threshold for historical lavas as determined by Paterson, 2011. The light red line is the inverse threshold value of $\vec{k}'$, −0.164, for specimens with concave-down Arai plots. Normalized intensity of 1.0, where the specimen estimate equals the expected field strength, is shown as a horizontal black dashed line. Arai plots for select specimens and their $\vec{k}'$ values are plotted in (b) hw2010Be, (c) hw126a5, and (d) hw126a2. (For interpretation of the references to color in this figure legend, the reader is referred to the web version of this article.)

are unsuitable for determining magnetic directions, paleointensity investigations will benefit if, where possible, researchers spend the requisite time collecting rapidly cooled material in addition to traditional drilling methods.

The success of our paleointensity experiments is impressive both in accuracy and consistency, six of our eight sampled lava flows yield statistically reliable results using very strict selection requirements. It is important to note that we require a minimum of three specimens per site with a standard deviation less than 10% of the mean. Most studies in the published literature ask for only two successful specimens per site and set a maximum standard deviation of 15% or greater. Each of our successful sites has at least four accepted specimens, which is a result of the single-domain-like material we collected for this study.

Paleointensity studies on rhyolitic volcanic glasses suggest that overestimates of 13% to 20% of ancient (Leonhardt et al., 2006) and experimental (Ferk et al., 2010) magnetic field strengths are likely to occur unless cooling rate corrections are performed. We find that cooling rate corrections on our modern glassy basalt specimens are unnecessary considering that our site results do not overestimate the magnetic field strength and actually (slightly) underestimate the field or reproduce the expected intensity within a 1σ-error, which is a few percent of the mean.

The benefits of using rapidly cooled material in paleointensity studies are demonstrated when comparing intensity results from the same historic lava flow. Fig. 7 plots individual paleointensity estimates from the 1960 Kilauea lava flow from the Big Island. All previously published studies in this figure used traditional drill

Table 4
Historic Hawaiian paleointensity results that meet our strict selection criteria. Field estimates derived from IZZI-modified Thellier–Thellier paleointensity experiments and calculated using the Thellier GUI Auto Interpreter. Listed beneath Lava Flow age is the expected field intensity, B_{exp}. B_F is the estimated field strength based on T °C temperature intervals. A_{Fac} is the ratio of anisotropy corrected/uncorrected intensity. Experimental statistics: *FRAC*, β, *MAD*, *DANG* and $\vec{k}'$.

Lava flow	Specimen	B_F	A_{Fac}	T °C	*FRAC*	β	*MAD*	*DANG*	$\vec{k}'$
1843	hw226a3	39.88	–	0–500	0.98	0.01	2.7	1.65	−0.02
B_{exp}=	hw226a5	35.33	–	0–275	0.88	0.04	2.61	0.55	0.15
39.2 μT	hw226b2	41.53	0.99	0–400	0.82	0.01	2.8	5.88	−0.04
	hw226b3	38.58	–	100–500	0.88	0.03	2.67	2.31	0.05
	hw226b6	40.64	–	0–375	0.78	0.02	1.8	5.91	0.05
	hw226 39.2 ± 2.4 μT, *n*=5								
1859	hw108a1	38.5	0.66	100–475	0.86	0.031	3.1	1.8	0.088
B_{exp}=	hw108a2	38.2	–	0–375	0.79	0.02	2	5.3	0.089
38.7 μT	hw108a5	41.8	–	100–450	0.87	0.014	0.7	1.1	−0.047
	hw108c1	40	–	100–350	0.86	0.015	0.4	1	0.074
	hw108c2	41.2	–	0–275	0.82	0.011	0.7	0.3	−0.018
	hw108c7	38.6	–	0–350	0.87	0.023	1.5	1.1	−0.008
	hw108c8	39.1	–	0–350	0.81	0.029	2.5	3.8	0.004
	hw108c9	37.8	–	0–500	0.99	0.015	1.9	0.8	−0.025
	hw108c12	34.4	–	100–375	0.8	0.059	1.5	0.9	0.074
	hw108c13	39.7	–	100–500	0.88	0.011	1.8	0.5	−0.017
	hw108 39.0 ± 2.0 μT, *n* = 10								
1907	hw123a1	33.3	–	0–510	0.97	0.0016	3.1	2.9	0.082
B_{exp}=	hw123a3	31.7	–	0–510	0.98	0.023	3.7	2.2	0
37.8 μT	hw123a4	35.3	–	0–510	0.96	0.034	1.5	0.5	−0.131
	hw123a9	90.2	–	150–500	0.81	0.052	3.4	1.2	0.033
	hw123 47.6 ± 28.4 μT, *n* = 4								
	hw123x 33.4 ± 1.8 μT, *n*=3								
1935	hw126a1	36.05	–	0–400	0.98	0.01	1.28	1.89	0.12
B_{exp}=	hw126a3	29.91	–	0–400	0.87	0.03	1.64	3.37	0.14
36.6 μT	hw126a4	37.04	–	100–375	0.78	0.02	1.9	3.6	0.11
	hw126a5	35.66	–	0–275	0.88	0	1.08	2.51	0.01
	hw126b1	35.64	–	100–425	0.84	0.02	1.04	1.26	0.06
	hw126b2	36.23	1.04	100–400	0.81	0.02	0.78	0.69	0.09
	hw126b3	35.6	–	0–425	0.97	0.01	0.83	1.12	0.06
	hw126b4	36.95	–	0–375	0.92	0.01	0.93	1.41	0.09
	hw126b5	36.52	–	0–375	0.92	0.01	0.51	0.42	0.02
	hw126 35.5 ± 2.2 μT, *n*=9								
1950	hw128a1	35.25	–	0–425	0.93	0.02	3.12	2.8	−0.06
B_{exp}=	hw128a2	37.42	–	100–510	0.89	0.02	1.43	1.72	0.14
36.3 μT	hw128a3	36.7	–	0–450	0.96	0.03	1.79	2.25	0.14
	hw128a4	36.13	–	100–510	0.93	0.02	0.76	1.19	0.12
	hw128a5	35.71	–	100–510	0.94	0.02	1.11	0.32	0.14
	hw128a6	36.6	–	100–500	0.87	0.04	1.62	2.52	0.08
	hw128a7	28.87	1.02	100–425	0.83	0.02	1.89	2.61	−0.14
	hw128a8	35.1	–	100–400	0.82	0.02	1.72	0.39	−0.12
	hw128a9	31.81	–	0–425	0.85	0.01	1.85	2.69	0.02
	hw128a10	32.01	1.06	100–425	0.87	0.02	1.86	2.78	−0.08
	hw128a11	44.25	–	100–500	0.94	0.02	2.14	2.26	0.15
	hw128b3	29.58	–	200–510	0.79	0.02	4.72	1.68	0.03
	hw128b4	31.04	–	200–510	0.88	0.02	2.88	0.79	0.06
	hw128b5	38.77	–	300–510	0.8	0.04	2.95	2.54	0.15
	hw128c1	34.02	1.06	0–510	1	0.01	2.27	0.75	0.05
	hw128c2	32.73	0.96	225–510	0.79	0.01	0.85	0.15	−0.12
	hw128c3	35.12	1.05	200–510	0.86	0.01	0.93	0.43	−0.01
	hw128c4	35.09	0.96	225–510	0.86	0.02	1.41	0.15	−0.05
	hw128c5	35.13	–	200–475	0.79	0.02	1.17	0.17	−0.08
	hw128d1	36.12	0.92	100–400	0.88	0.02	2.23	2.72	0.06
	hw128d2	34.78	1.01	0–450	0.97	0.03	1.55	2.59	0.08
	hw128d3	35.49	–	0–425	0.92	0.04	1.72	4.95	0.1
	hw128d4	33.59	–	0–350	0.8	0.02	1.47	1.68	−0.1
	hw128 34.8 ± 3.2 μT, *n*=23								
1960	hw241a2	31.21	–	150–500	0.8	0.02	4.06	1.33	−0.03
B_{exp}=	hw241d3	41.39	–	275–500	0.79	0.02	4.79	2.1	0.1
36.2 μT	hw241e1	36.29	1.01	0–425	0.84	0.03	2.27	3.73	−0.1
	hw241e2	36.94	–	100–475	0.85	0.02	2.68	2.95	0.16
	hw241e4	37.82	1.02	100–500	0.78	0.01	2.77	3.68	−0.01
	hw241e5	34.41	–	0–500	0.98	0.02	2.83	2.13	0.14
	hw241e6	33.92	–	0–425	0.86	0.04	2.54	2.48	0.02
	hw241 36.0 ± 3.2 μT, *n*=7								
1990	hw201a3	34.31	–	0–325	0.79	0.03	2.68	8.79	0.16
B_{exp}=	hw201a6	33.13	–	0–450	0.9	0.02	2.37	1.58	0.16
35.4 μT	hw201a11	31.59	–	0–400	0.81	0.03	3.34	1.37	0.16
	hw201a12	31.83	–	0–450	0.79	0.02	2.78	7.69	0.12
	hw201 32.7 ± 1.26 μT, *n* = 4								

Table 5
Site level paleointensity results using strict selection criteria for historic Hawaiian lava flows including the application of the $\vec{k}'$ criterion. B_F is the estimated ancient field strength in microTesla, B_σ is the standard deviation of each sample field estimate and B_σ % is percent error of each estimate. B_{exp} is the expected intensity for each lava, ΔB is the difference between the estimated and expected field strengths, ΔB% is the percent difference.

Lava flow	Site name	n	B_F (μT)	B_σ	B_σ %	B_{exp} (μT)	ΔB	ΔB%
With $\lvert\vec{k}'\rvert$ criterion								
1843	hw226	6	39.2	2.4	6.1	39.2	0.0	0.0
1859	hw108	10	39	2.0	5.1	38.7	0.3	0.8
1935	hw126	9	35.5	2.2	6.2	36.6	−1.1	−3.0
1950	hw128	23	34.8	3.2	9.2	36.3	−1.5	−4.1
1960	hw241	7	36	3.2	8.9	36.2	−0.2	−0.6
1990	hw201	4	32.7	1.3	4.0	35.4	−2.7	−7.6

cores or subsampled larger hand samples from the basaltic lava flow interior, whereas we sampled the rapidly cooled flow tops. In this figure, the most recent publications have less variation and greater accuracy than earlier intensity studies. A dramatic reduction in variance is especially evident for those studies using Thellier-type paleointensity experiments. Part of the reason for this improvement can be attributed to observations of positive correlations between NRM fraction (Chauvin et al., 2005), unblocking temperature spectra (Herrero-Bervera and Valet, 2009) and paleointensity success. A general trend towards stricter acceptance criteria also limits the inclusion of imperfect experimental results and removes the need to interpret subjective Arai diagrams caused by multi-domain-like behavior.

We tested whether our successful recovery of the 1960 Hawaiian field intensity can be duplicated on samples collected from the slowly-cooled interior of the flow. Yamamoto et al. (2003) applied the Coe-Thellier intensity experiment (Coe, 1967) to 19 samples drilled out of the 1960 Kilauea flow and found that 17 passed their selection requirements (a slightly modified version of those used by Coe et al. (1978)). The mean intensity of those specimens (49.0 ± 9.6 μT) is about 35% higher than the expected field strength. When we apply our strict specimen selection criteria to the raw measurement data from Yamamoto et al. (2003) (available for download from the MagIC database at: http://earthref.org/MagIC/9552), we find that the average intensity from eight accepted specimens, 39.1 ± 5.0 μT, is within one standard deviation of the expected value. The improvement in mean intensity for the Yamamoto et al. (2003) dataset can be attributed to the removal of nine specimens with curved Arai plots that had an original range of calculated intensities between 45 and 85 μT. The high intensities of these now rejected specimens could be the result of TCRM acquisition during lava emplacement as suggested by Yamamoto (2006) and may also be a function of the steeper, low temperature Arai plot component chosen for intensity calculation. The revised results of the Yamamoto et al. (2003) data is certainly an improvement over the original site average, but this new dataset would not pass our site requirement that the standard deviation of all accepted specimens be within 4 μT or 10% of the mean. The reasons for this higher variance, compared to the results from our data from rapidly cooled specimens, could be due to the difference in sample material or perhaps the different experimental techniques. We note that the traditional Coe-variant of the method does not test for the equivalence of unblocking and blocking temperatures (a symptom of non-single domain behavior) so is less sensitive in detecting unsuitable material.

The benefit of volcanic glass as an experimental material is that a greater percentage of measured specimens will be single-domain, therefore the likelihood of a successful experiment will increase and time consuming thermal heating experiments will be more fruitful. In some instances however, even apparently ideal specimens can differ by 20% of the expected intensity (e.g. Fig. 4). Multi-domain specimens generally yield curved Arai plots and are unreliable recorders of paleointensity as they are subject to multiple slope interpretations and consistently underestimate the ancient field strength when taking the full TRM. Our preference for sampling glassy material limits the amount of multi-domain material in our collection and therefore the number of specimens requiring subjective interpretations. There is little question about what a 'perfect' experimental result looks like, and we are fortunate that approximately half of our measured specimens closely

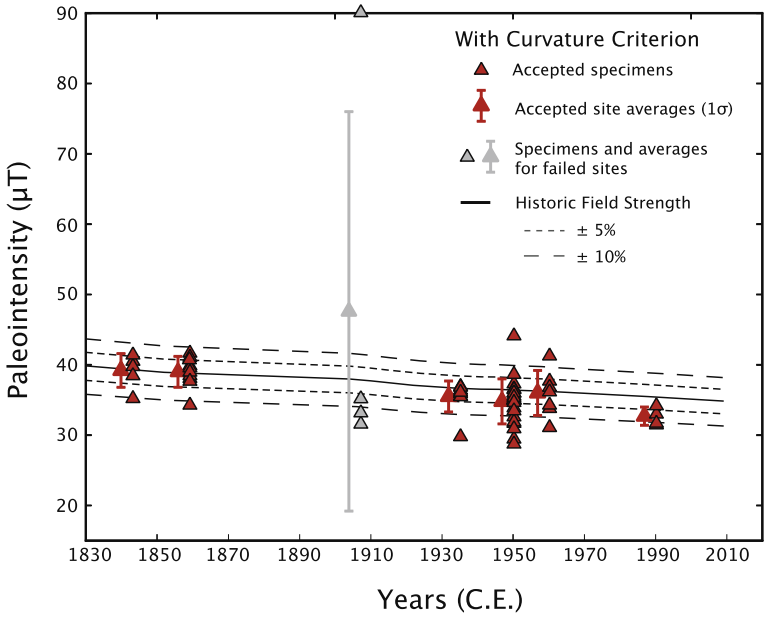

Fig. 6. Strict paleointensity results for historical Hawaiian lavas calculated with the additional $|\vec{k}'|$ constraint. Accepted specimens are plotted as red triangles, site averages and 1σ-error bars are offset. Failed sites and specimens are plotted in gray. The solid line is the historical field strength on the Big Island of Hawaii, dashed lines are ±5% and 10% of the expected field. Hawaiian field strength calculated from D/IGRFs for 1900 to 2010 C.E. (Malin and Barraclough, 1981), prior to 1900 C.E. calculated from ARCH3K.1 (Korte et al., 2009). Field strength values were generated using igrf.py (part of Lisa Tauxe's PmagPy package).

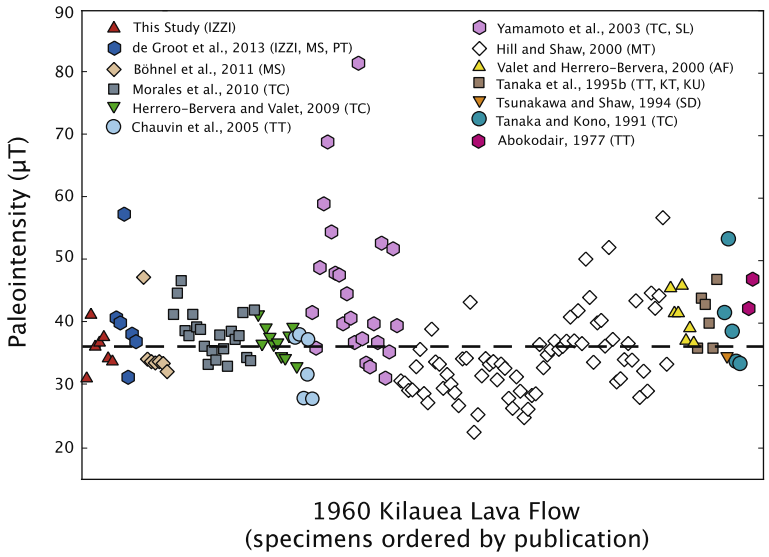

Fig. 7. Specimen level paleointensity estimates for the 1960 Kilauea flow from this study (red triangles) and published literature. 1960 C.E. IGRF field strength at the Big Island is 36.1 μT (dashed line). Preferred results, as determined by the authors of each study, are plotted by publication year, with our results on the far left and progressively older studies to the right. Paleointensity experiment codes: IZZI = IZZI-modified Thellier (Tauxe and Staudigel, 2004); MS = Multispecimen, domain-state-corrected (Deckers and Böhnel, 2006); PT = Pseudo-Thellier (Tauxe et al., 1995); TC = Coe Thellier (Coe, 1967); TT = Thellier–Thellier (Thellier and Thellier, 1959); SL = Shaw Low Temperature Demagnetization-Double Heating Technique (Tsunakawa et al., 1997; Tsunakawa et al., 1997); MT = Microwave Thellier (Hill and Shaw, 1999); AF = Alternating Field (Van Zijl et al., 1962); KT = Königsberger Thellier (Königsberger, 1938); KU = Kono and Ueno (Kono and Ueno, 1977); SD = Shaw Double Heating (Tsunakawa and Shaw, 1994). (1960 Kilauea flow studies not cited elsewhere in this manuscript: Abokodair, 1977; Böhnel et al., 2011; Hill and Shaw, 2000; Morales et al., 2010; Tanaka and Kono, 1991; Valet and Herrero-Bervera, 2000).

follow Néel theory and produce nearly linear Arai plots and single-domain like behavior.

Curvature calculation of Thellier-type experiments and implementation of the $|\vec{k}'|$ threshold complements our optimized selection criteria by identifying non-ideal specimens that underestimate the expected field strength due to effects from multi-domain grains. The addition of $|\vec{k}'|$ removes a low-field bias in our specimens and should be used as an additional selection statistic in future paleointensity studies.

While Fig. 7 illustrates a general trend towards greater sample accuracy, it also highlights the inherent uncertainty of existing paleointensity estimates in the literature. The inability of researchers to consistently recover the magnetic field strength of lavas extruded in known fields is troubling, considering that essentially all specimens in the published literature were erupted in unknown fields. Except for rare instances, specimens with a linear Arai plot can be expected to accurately record the ancient field strength, regardless of the type of material being used (e.g., volcanic glass or crystalline interior), however much of the published data is non-ideal. In order to remove the effect of deviant field estimates, stricter criteria must be used especially at the sample level. We have shown that the expected magnetic field strength can be recovered within 8% (4% when using the $\vec{k}'$ criterion) using at least four specimens per site. Requiring three or four individual estimates (or more) per site reveals within-site discrepancies and will allow researchers to better constrain changes in the geomagnetic field.

It is reasonable to suggest that the variance observed in Fig. 7 is representative of all published intensity data, and the distribution would suggest that acquiring an accurate estimate of geomagnetic field strength will be difficult over an given time interval. We use the published intensity values from all 1960 Kilauea specimens in Fig. 7 to determine if it is possible to use published intensity data to obtain accurate field strength estimates for a single location at a given point in time (e.g., 1960 C.E. in Hawaii, see Fig. 8a) and over an average of 5 millions years (Fig. 8b). Fig. 8a shows the deviation of average paleointensity estimates for a variable number of n specimens. For each n, specimens are randomly drawn from the published 1960 Kilauea data set (Fig. 7) and averaged together. This procedure is performed 10,000 times and the median field estimate and bootstrapped 95% confidence intervals are calculated. The skewed data distribution of the 1960 flow towards higher than expected intensities is reflected in the median intensities for each n; median bootstrap values overestimate the expected field strength by a few μT (1.6 μT for $n = 2$, 2.7 μT for $n = 100$) but are within 95% confidence of the true field until about $n = 30$. The simulation results in Fig. 8a suggest that any intensity estimate derived from published data at a given site is likely to overestimate the field by 1.6–2.7 μT or 4.5–7.5% of the expected Hawaiian intensity.

Next, we test whether the variabilities in site level estimates observed in Fig. 8a affect long-term calculations of field strength. In Fig. 8b we present median paleointensity estimates for a parameterized set of field vectors drawn from PSV model TK03 (Tauxe and Kent, 2004) at the 1960 Kilauea flow site (19.52°N, −154.81°E). The median intensity of N sites was calculated by randomly selecting N full-field vectors from TK03 (out of a possible 10,000) and redetermining the intensity by averaging n randomly drawn values from a distribution about the selected vector, where the variance about each vector is the 95% confidence distribution of n determined in Fig. 8b. This calculation is performed 10,000 times for each set of N estimates. The median intensity of the generated TK03 field vectors is 21.3 μT, which represents the expected long-term intensity at Hawaii over the last 5 million years. Our parametric bootstrap simulations suggest that any long-term field estimate is very likely to overestimate the actual paleointensity, regardless of the number of sites used in the calculation. The bootstrapped intensity values approach the expected field strength with increasing n, while the variance in field estimates is a function of N. Not surprisingly, a higher N and n will result in a more precise and accurate intensity calculation.

Finding a large number of sites in the literature from a single location is difficult as very few sites in the published data have an n of 10. Most paleointensity sites are averages of between two

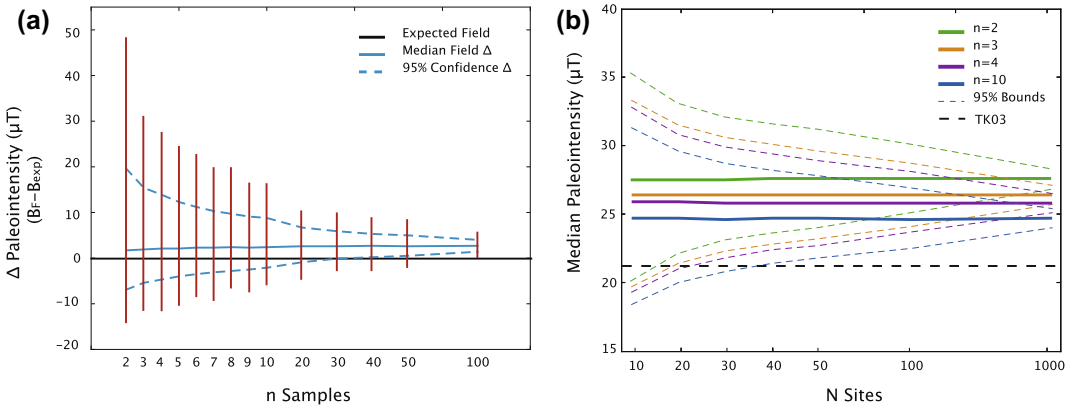

Fig. 8. Simulated paleointensity results drawn from published 1960 Kilauea lava flow data. (a) Deviation of average paleointensity estimates for variable *n* specimens. Red lines show the distribution of the bootstrapped averages of each *n*, dashed blue lines are the 95% confidence interval and the solid blue line is the median field estimate of each *n* distribution. (b) Median paleointensity estimates for a parameterized set of field vectors drawn from TK03 (Tauxe and Kent, 2004) at the 1960 Kilauea flow site (19.52°N, −154.81°E). Solid lines are the median intensity results for each *N*, and dashed lines are the 95% confidence interval. The black dashed line is the median intensity of all TK03 field vectors. (For interpretation of the references to color in this figure legend, the reader is referred to the web version of this article.)

and four specimens which, according to our simulations, would overestimate the geomagnetic field strength by 4.5–6.2 μT, or about 20–30% of the field in Hawaii. These simulations are based on the assumption that the uncertainty in site level paleointensity estimates is similar to what is observed at the 1960 Kilauea lava flow, which would lead to overestimates of the expected field. The use of strict selection criteria and rapidly cooled volcanic material in experimental analysis can reliably approximate the expected field intensity and reduce the site level variance to under 10%. Until such time as reliable estimates of unknown geomagnetic field strengths can be consistently recovered, long-term paleointensity calculations are likely to overestimate the true value by perhaps as much as 25%.

5. Conclusion

Subaerial basaltic volcanic glass is an accurate recorder of magnetic field strength when measured using the IZZI-modified Thellier-type experiment. We obtained successful results from six historic lava flows on the Big Island of Hawaii (1843, 1859, 1935, 1950, 1960, 1990 C.E.) using a strict set of selection requirements. Five flows have an average field intensity within 4% of the expected field and all but one (1990 C.E.) are within 1σ-error of the actual intensity. The 1990 flow underestimated the expected field strength by 8%, which is only 2.7 μT away from the known field.

Published sample intensities from the 1960 Kilauea lava flow are not normally distributed and likely to result in an overestimate of the expected field strength. This skewed distribution of site level calculations are therefore likely to produce overestimates of the long-term geomagnetic field, perhaps as much as 25%.

Paleointensity experiments on lava flows can be precise and accurate when the proper material is collected and strict selection criteria are applied. The success of this study in reproducing the Earth's magnetic field strength can be attributed to our stringent statistical requirements and the use of glassy material from lava flow tops. Rapidly cooled volcanics are more likely to be single-domain and behave according to paleomagnetic theory during repeat heating experiments. The use of ideal material in paleointensity investigations allows for objective interpretations of Arai diagrams and simplifies the data analysis process. Volcanic glass may not be present in all geologic settings and can be difficult to identify in the field, but we encourage future expeditions to collect rapidly cooled (micro-crystalline) samples for paleointensity research.

Acknowledgments

We are especially grateful to Ron Shaar for his insightful comments and helpful discussions and help with measurements of the 2010 lava flow specimens. Many thanks to Greig Paterson for his very helpful review and for sharing his curvature code during initial processing of the data. We thank Cathy Constable, Jeff Gee, Tom Levy and Catherine Johnson for their helpful comments, and to one anonymous reviewer for their input. Thanks to Jason Steindorf and Miranda Mikesh for assistance in sample preparation and laboratory analysis. This work was funded by NSF: EAR114840 (LT) and BSF: 2008198 (LT and HR).

References

Abokodair, A., 1977. The Accuracy of the Thelliers Technique for the Determination of Paleointensities of the Earth's Magnetic Field. PhD Thesis, University of California Santa Cruz.

Aitken, M., Allsop, A., Bussell, G., Winter, M., 1988. Determination of the intensity of the Earth's magnetic field during archaeological times: Reliability of the Thellier technique. Rev. Geophys. 26 (1), 3–12.

Biggin, A., Steinberger, B., Aubert, J., Suttie, N., Holme, R., Torsvik, T., van der Meer, D., van Hinsbergen, D., 2012. Possible links between long-term geomagnetic variations and whole-mantle convection processes. Nat. Geosci. 5, 526–533.

Böhnel, H., Herrero-Bervera, E., Dekkers, M., 2011. Paleointensities of the Hawaii 1955 and 1960 lava Flows: further validation of the multi-specimen method. In: Petrovsky, E., Herrero-Bervera, E., Harinarayana, T., Ivers, D. (Eds.), Earth's Magnetic Interior, vol. 1, pp. 195–211.

Bowles, J., Gee, J., Kent, D., Perfit, M., Soule, S., Fornari, D., 2006. Paleointensity applications to timing and extent of eruptive activity, 9°–10°N East Pacific Rise. Geochem. Geophys. Geosyst. 7 (6).

Chauvin, A., Roperch, P., Levi, S., 2005. Reliability of geomagnetic paleointensity data: the effects of the NRM fraction and concave-up behavior on paleointensity determinations by the Thellier method. Phys. Earth Planet. Inter. 150, 265–286.

Chernov, N., Lesort, C., 2005. Least squares fitting of circles. J. Math. Imaging Vision 23, 239–252.

Coe, R., 1967. Paleo-intensities of the Earth's magnetic field determined from tertiary and quaternary rocks. J. Geophys. Res. 72 (12), 3247–3262.

Coe, R.S., Grommé, S., Mankinen, E.A., 1978. Geomagnetic paleointensities from radiocarbon-dated lava flows on Hawaii and the question of the Pacific nondipole low. J. Geophys. Res. 83, 1740–1756.

Cromwell, G., Tauxe, L., Staudigel, H., Constable, C., Koppers, A., Pedersen, R.-B., 2013. In search of long term hemispheric asymmetry in the geomagnetic field: results from high northern latitudes. Geochem. Geophys. Geosyst. 14 (8).

Day, R., Fuller, M., Schmidt, V., 1977. Hysteresis properties of titanomagnetites: grain size and composition dependence. Phys. Earth Planet. Inter. 13 (260–266).

Deckers, M., Böhnel, H., 2006. Reliable absolute paleointensities independent of magnetic domain state. Earth Planet. Sci. Lett. 248, 508–517.

de Groot, L., Biggin, A., Dekkers, M., Langereis, C., Herrero-Bervera, E., 2013. Rapid regional perturbations to the recent global geomagnetic decay revealed by a new Hawaiian record. Nat. Commun. 4.

Dunlop, D., Özdemir, O., 2001. Beyond Néel's theories: thermal demagnetization of narrow-band partial thermoremanent magnetization. Phys. Earth Planet. Inter. 126, 43–57.

Ferk, A., Aulock, F.W.v., Leonhardt, R., Hess, K.-U., Dingwell, D., 2010. A cooling rate bias in paleointensity determination from volcanic glass: An experimental demonstration. J. Geophys. Res. 115 (B08102).
Ferk, A., Leonhardt, R., Hess, K.-U., Dingwell, D., 2011. Paleointensities on 8 ka obsidan from Mayor Island, New Zealand. Solid Earth 2, 259–270.
Ferk, A., Denton, J., Leonhardt, R., Tuffen, H., Koch, S., Hess, K.-U., Dingwell, D., 2012. Paleointensity on volcanic glass of varying hydration states. Phys. Earth Planet. Inter. 208–209, 25–37.
Harrison, R., Feinberg, J., 2008. An improved algorithm for calculating first-order reversal curve distributions using locally weighted regression smoothing. Geochem. Geophys. Geosyst. 9.
Herrero-Bervera, E., Valet, J.P., 2009. Testing determinations of absolute paleointensity from the 1955 and 1960 Hawaiian flows. Earth Planet. Sci. Lett. 287, 420–433.
Hext, G., 1963. The estimation of second-order tensors, with related tests and designs. Biometrika 50, 353–357.
Hill, M., Shaw, J., 1999. Palaeointensity results for historic lavas from Mt. Etna using microwave demagnetization/remagnetization in a modified Thellier-type experiment. Geophys. J. Int. 139, 583–590.
Hill, M., Shaw, J., 2000. Magnetic field intensity study of the 1960 Kilauea lava flow, Hawaii, using the microwave palaeointensity technique. Geophys. J. Int. 142, 487–504.
Hoffman, K., Biggin, A., 2005. A rapid multi-sample approach to the determination of absolute paleointensity. J. Geophys. Res. 110, B12108.
Hoffman, K., Constantine, V., Morse, D., 1989. Determination of absolute palaeointensity using a multi-specimen procedure. Nature 339, 295–297.
Jackson, A., Jonkers, A.R.T., Walker, M.R., 2000. Four centuries of geomagnetic secular variation from historical records. Philos. Trans. R. Soc. Lond. Ser. A 358 (1768), 957–990.
Jelinek, V., 1978. Statistical processing of anisotropy of magnetic-susceptibility measured on groups of specimens. Stud. Geophys. Geodyn. 22, 50–62.
Kirschvink, J.L., 1980. The least-squares line and plane and the analysis of paleomagnetic data. Geophys. J. R. Astron. Soc. 62, 699–718.
Königsberger, J., 1938. Natural residual magnetism of eruptive rocks. Terr. Magn. Atmos. Electr. 43 (119–127), 299–320.
Kono, M., Ueno, N., 1977. Paleointensity determination by a modified Thellier method. Phys. Earth Planet. Inter. 13, 305–314.
Korte, M., Donadini, F., Constable, C., 2009. Geomagnetic field for 0–3 ka: 2. A new series of time-varying global models. Geochem. Geophys. Geosyst. 10 (6).
Leonhardt, R., Matzka, J., Nichols, A., Dingwell, D., 2006. Cooling rate correction of paleointensity determination for volcanic glass by relaxation geospeedometry. Earth Planet. Sci. Lett. 243, 282–292.
Levi, S., 1977. The effect of magnetite particle size on paleointensity determinations of the geomagnetic field. Phys. Earth. Planet. Inter. 13, 245–259.
Love, J., Constable, C., 2003. Gaussian statistics for palaeomagnetic vectors. Geophys. J. Int. 152, 515–565.
Malin, S., Barraclough, D., 1981. An algorithm for synthesizing the geomagnetic field. Comput. Geosci. 7, 401–406.
Morales, J., Zhao, X., Goguitchaichvili, A., 2010. Geomagnetic field intensity from Kilauea 1955 and 1960 lava flows: towards a better understanding of paleointensity. Stud. Geophys. Geodyn. 54, 561–574.
Nagata, T., Arai, Y., Momose, K., 1963. Secular variation of the geomagnetic total force during the last 5000 years. J. Geophys. Res. 68, 5277–5282.
Paterson, G., 2011. A simple test for the presence of multidomain behavior during paleointensity experiments. J. Geophys. Res. 116, B10104.
Paterson, G., 2013. The effects of anisotropic and non-linear thermoremanent magnetizations on Thellier-type paleointensity data. Geophys. J. Int. 193, 694–710.
Paterson, G., Biggin, A., Yammamoto, Y., Pan, Y., 2012. Towards the robust selection of Thellier-type paleointensity data: the influence of experimental noise. Geochem. Geophys. Geosyst. 13 (5).
Paterson, G., Tauxe, L., Biggin, A., Shaar, R., Jonestrask, L., 2014. On improving the selection of Thellier-type paleointensity data. Geochem. Geophys. Geosyst. 15, 1180–1192.
Pick, T., Tauxe, L., 1993. Holocene paleointensities: Thellier experiments on submarine basaltic glass from the East Pacific Rise. J. Geophys. Res. 98 (B10), 17949–17964.
Shaar, R., Feinberg, J., 2013. Rock magnetic properties of dendrites: insights from MFM imaging and implications for paleomagnetic studies. Geochem. Geophys. Geosyst. 14 (2).
Shaar, R., Tauxe, L., 2013. Thellier Gui: an integrated tool for analyzing data from Thellier-type experiments. Geochem. Geophys. Geosyst. 14 (3).
Shaw, J., 1974. A new method of determining the magnitude of the paleomagnetic field application to 5 historic lavas and five archeological samples. Geophys. J. R. Astron. Soc. 39, 133–141.
Tanaka, H., Kono, M., 1991. Preliminary results and reliability of palaeointensity studies on historical and C^{14} dated Hawaiian Lavas. J. Geomagn. Geoelectr. 43, 375–388.
Tanaka, H., Kono, M., Uchimura, H., 1995. Some global features of palaeointensity in geological time. Geophys. J. Int. 120, 97–102.
Tarduno, J., Cottrell, R., Watkeys, M., Hofmann, A., Doubrovine, P., Mamajek, E., Liu, D., Neukirch, L., Usui, Y., 2010. Geodynamo, solar wind, and magnetopause 3.4 to 3.45 billion years ago. Science 327, 1238–1240.
Taubin, G., 1991. Estimation of planar curves, surfaces, and nonplanar space curves defined by implicit equations with applications to edge and range image segmentation. IEEE Trans. Pattern Anal. Mach. Intell. 13, 1115–1138.
Tauxe, L., Kent, D.V., 2004. A simplified statistical model for the geomagnetic field and the detection of shallow bias in paleomagnetic inclinations: was the ancient magnetic field dipolar? In: Channell, J.E.T.e.a. (Ed.), Timescales of the Paleomagnetic Field, vol. 145. American Geophysical Union, Washington, D.C., pp. 101–116.
Tauxe, L., Staudigel, H., 2004. Strength of the geomagnetic field in the cretaceous normal Superchron: new data from submarine basaltic glass of the Troodos Ophiolite. Geochem. Geophys. Geosyst. 5 (2), Q02H06. http://dx.doi.org/10.1029/2003GC000635.
Tauxe, L., Yamazaki, T., 2007. Paleointensities. In: Kono, M. (Ed.), Geomagnetism, Vol. 5 of Treatise on Geophysics. Elsevier, pp. 509–563. http://dx.doi.org/10.1016/B978-044452748-6/00098-5.
Tauxe, L., Pick, T., Kok, Y., 1995. Relative paleointensity in sediments: a pseudo-Thellier approach. Geophys. Res. Lett. 22 (21), 2885–2888.
Tauxe, L., Banerjee, S., Butler, R., van der Voo, R., 2010. Essentials of Paleomagnetism. University of California Press.
Thellier, E., Thellier, O., 1959. Sur l'intensité du champ magnétique terrestre dans le passé historique et géologique. Ann. Geophys. 15, 285–378.
Tsunakawa, H., Shaw, J., 1994. The Shaw method of palaeointensity determinations and its application to recent volcanic rocks. Geophys. J. Int. 118, 781–787.
Tsunakawa, H., Shimura, K., Yammamoto, Y., 1997. Application of a Double Heating Technique of the Shaw Method to the Brunhes Epoch Volcanic Rocks (Abstract). 8th Scientific Assembly IAGA, Uppsala.
Valet, J.-P., Herrero-Bervera, E., 2000. Paleointensity experiments using alternating field demagnetization. Earth Planet. Sci. Lett. 177, 43–58.
Van Zijl, J., Graham, K., Hales, A., 1962. The paleomagnetism of the Stromberg lavas of South Africa, II. The behaviour of the northern magnetic field during a reversal. Geophys. J. R. Astron. Soc. 7, 169–182.
Veitch, R., Hedley, I., Wagner, J., 1984. An investigation of the intensity of the geomagnetic-field during Roman times using magnetically anisotropic bricks and tiles. Arch. Sci. 37, 359–373.
Wang, H., Kent, D., 2013. A paleointensity technique for multidomain igneous rocks. Geochem. Geophys. Geosyst. 14.
Yamamoto, Y., 2006. Possible TCRM acquisition of the Kilauea 1960 lava, Hawaii: failure of the Thellier paleointensity determination inferred from equilibrium temperature of the Fe–Ti oxide. Earth Planets Space 58, 1033–1044.
Yamamoto, Y., Tsunakawa, H., Shibuya, H., 2003. Palaeointensity study of the Hawaiian 1960 lava: implications for possible causes of erroneously high intensities. Geophys. J. Int. 153, 263–276.
Ziegler, L., Constable, C., Johnson, C.L., Tauxe, L., 2011. PADM2M: a penalized maximum likelihood model of the 0–2 Ma palaeomagnetic axial dipole moment. Geophys. J. Int..
Zijderveld, J., 1967. A.C. demagnetization of rocks: analysis of results. Methods Paleomagnetism, 254–286.